ADVANCED MATERIALS
www.advmat.de

# Fluoropolymer Nanosheet as a Wrapping Mount for High-Quality Tissue Imaging

*Hong Zhang, Ami Masuda, Ryosuke Kawakami, Kenji Yarinome, Riku Saito, Yu Nagase, Tomomi Nemoto, and Yosuke Okamura**

**In the field of biological microscopy technology, it is still a practical challenge to obtain high-quality tissue images, due to the tissue desiccation that occurs during observations without an effective sample mounting. Inspired by the use of plastic food wrap, this study proposes the use of polymer thin films (also known as nanosheets) to fix the tissue samples. Water-repellent nanosheets composed of the amorphous fluoropolymer CYTOP are prepared with adjustable thicknesses and their hydrophobicity, transparency, and adhesion strength are evaluated. They show excellent water-retention effect and work well for sample fixation. By wrapping cleared mouse brain slices with a 133 nm thick CYTOP nanosheet, this study achieves high spatial resolution neuron images while scanning over a large area for a long period of time. No visible artifacts arising from sample shrinkage can be detected. This study also expects that nanosheet wrapping could be effective over a longer time span by combination with conventional agarose embedding.**

High-quality visualization of organisms and tissues can provide a powerful approach to understand cellular functions in a systematic manner. Over the past decade, a number of developments in microscopy have been made, such as two-photon (TP) excitation microscope, light sheet microscopy (LSFM/SPIM), total internal reflection fluorescence microscope (TIRF), stimulated emission depletion microscope (STED), stochastic optical reconstruction microscope (STORM), photoactivation localization microscope (PALM), etc.[1] These state-of-the-art microscopy techniques now enable us to image living tissues in three dimensions with a high resolution at a fast speed. Very recently, various optical clearing agents that make treated tissues transparent have also been reported, which might ultimately allow tissue imaging to reach a deeper location.[2] Most technical limitations seem to have been overcome; however, to obtain acceptable tissue images remains a practical challenge.

A critical role of mounting is to maintain the physiological environment of tissue samples during observation. In traditional wet mount, to prevent evaporation of the medium, a cover slip is placed on the top of the sample, and the adding of a cover slip may squash the fragile tissues. An alternative method for mounting tissues is agarose embedding.[3] While not completely eliminating crushing, agarose mounting can reduce the crushing problem, but this method increases the background level and deteriorates the quality of phase contrast. In both cases, the shrinkage of tissue samples for a long-time imaging is always inevitable. Sample desiccation can cause undesirable movements on the microscopy stage, posing serious problems for stable imaging. Various closed chambers have been developed to lengthen the observation time for imaging. In a practical tissue imaging task, however, chambers with function of environmental control must be specifically designed according to the size and type of tissue samples, which always causes a high cost of chambers and is still reliant much on the know-how of researchers.[4] Compared to the rapid development of microscopy, the improvement of sample mounting techniques is very limited and a versatile mounting strategy giving excellent water retention effect for sample fixation is highly desirable.

Much attention has been recently paid to fabrication of polymer thin films (thickness of ≈100 nm, also known as nanosheets) as novel nanomaterials for biomedical applications owing to their unique properties, such as a high level of flexibility, adhesion strength, and transparency.[5] With freestanding procedures, nanosheets can be detached from their prepared solid substrate and transferred to any other surface, such as human skin and animal organs. In our previous studies, biodegradable nanosheets composed of poly(L-lactic acid) (PLLA) with many configurations, such as monolayer, multilayer, and fragments have been fabricated, and their potentials as in vivo glue-free wound dressing materials and drug deliver carriers have been demonstrated.[5] Here, to address the issue of sample mounting for tissue imaging, the use of plastic wrap

Dr. H. Zhang, Dr. Y. Okamura
Micro/Nano Technology Center
Tokai University
4-1-1 Kitakaname, Hiratsuka, Kanagawa 259-1292, Japan
E-mail: y.okamura@tokai-u.jp
A. Masuda, K. Yarinome, R. Saito, Prof. Y. Nagase, Dr. Y. Okamura
Department of Applied Chemistry
School of Engineering
Tokai University
4-1-1 Kitakaname, Hiratsuka, Kanagawa 259-1292, Japan
Dr. R. Kawakami, Prof. T. Nemoto
Research Institute for Electronic Science
Graduate School of Information Science and Technology
Hokkaido University
Kita 20 Nishi 10, Kita-ku, Sapporo 001-0020, Japan

**DOI: 10.1002/adma.201703139**

 

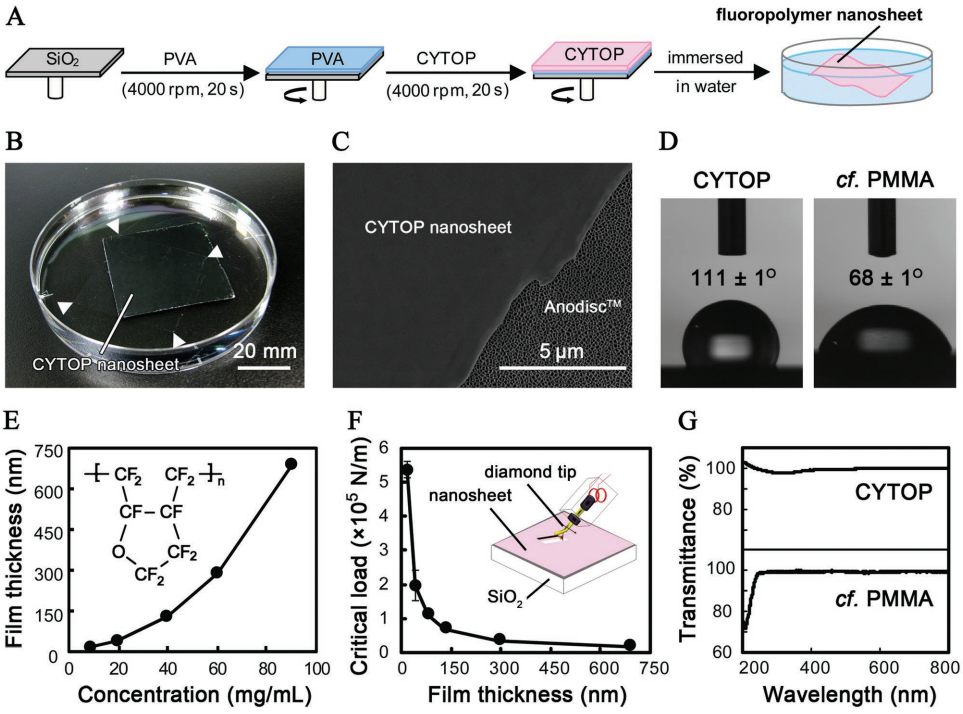


**Figure 1.** Fabrication of fluoropolymer nanosheet. A) Schematic representation of fabrication of a freestanding CYTOP nanosheet using a spin-coating and PVA sacrificial layer method. B) Macroscopic image of a CYTOP nanosheet with a thickness of 133 nm floated on the surface of water (arrows show the corner of the nanosheet). C) SEM image of a CYTOP nanosheet adhered on an Anodisc membrane. D) Static water contact angle of CYTOP and PMMA nanosheets with a similar thickness of 133 nm. E) Correlation between the thickness of CYTOP nanosheet and the concentration of coating solution (insert shows the structural formula of CYTOP). F) Critical load for detachment of the CYTOP nanosheet re-supported on a $SiO_2$ substrate (insert schematically shows the scratch tester, where a diamond tip scratches the nanosheet surface). G) Transmittance in the wavelength range from 200 to 800 nm of CYTOP and PMMA nanosheets with a similar thickness of 295 nm.

for sealing food in our daily life inspired us. If we could wrap tissue samples with nanosheets that have restricted water permeability and strong adhesion, such a mount may satisfy the above requirements.

The water permeability through a polymer film is dependent on the polarity of the polymer. The solubility of water in a hydrophobic film is negligible due to their low thermodynamic compatibility, and thus the water permeation is very restricted.[6] It is known that Teflon is often employed to give a water-repellent coating. Among numerous existing fluoropolymers, perfluoro(1-butenyl vinyl ether) polymer (commercially known as CYTOP) offers good room temperature solubility and coatability.[7] Compared to partially crystalline Teflon, CYTOP is amorphous, mechanically durable, stiff (Young's modulus = 1.4–1.6 GPa) and stretchable (elongation at break ≅ 150%). Besides, CYTOP has a high optical transmittance, with a glass transition temperature of 108 °C, while maintaining a similar low surface energy (19 mN $m^{-1}$). Thanks to these properties, CYTOP has shown its superiority in building functional surfaces for controlling nonspecific protein binding, gate dielectrics for organic field-effect transistors, transparent windows for liquid microlenses, etc.[8] However, there has been no report on material design that can combine the characteristics of CYTOP and the advantages of a nanosheet configuration.

Here, we report the fabrication of CYTOP fluoropolymer nanosheets and evaluate their hydrophobicity, transparency, and adhesive strength. A nanosheet wrapping mount is proposed, and its water retention effect is demonstrated. We also present the first attempt to image nanosheet-wrapped mouse brain slices for a long scan time over a large area at high spatial resolution and identifiability.

First, freestanding CYTOP nanosheets were fabricated as shown in **Figure 1**A. Poly(vinyl alcohol) (PVA) as a water-soluble sacrificial layer was previously spin-coated onto a $SiO_2$ substrate. CYTOP dissolved in perfluorotributylamine (PFTBA) at a variety of concentrations was subsequently coated. When the substrate was immersed in water, the CYTOP nanosheet detached from the substrate and floated spontaneously on the surface of water due to the dissolution of the PVA layer (≈15 nm thickness). CYTOP has a refractive index of 1.34, which is similar to that of water, and thus the edge of a CYTOP nanosheet is almost invisible (Figure 1B). Due to the water-repellency of CYTOP, the floating nanosheet did not sink even after adding surfactant into the water (data not shown). Observation of a CYTOP nanosheet on an Anodisc membrane using a scanning electron microscope (SEM) confirmed that the surface of the nanosheet was flat and uniform without any cracks or wrinkles (Figure 1C). The static water contact angle of a CYTOP nanosheet was measured to be 111 ± 1°, which is much larger than that of poly(methyl methacrylate) (PMMA, 68 ± 1°), a common amorphous acrylic-glass (Figure 1D). CYTOP nanosheets were next resupported on $SiO_2$ substrates and the film thickness was analyzed with a stylus profilometer. The thickness of CYTOP nanosheets was proportional to the

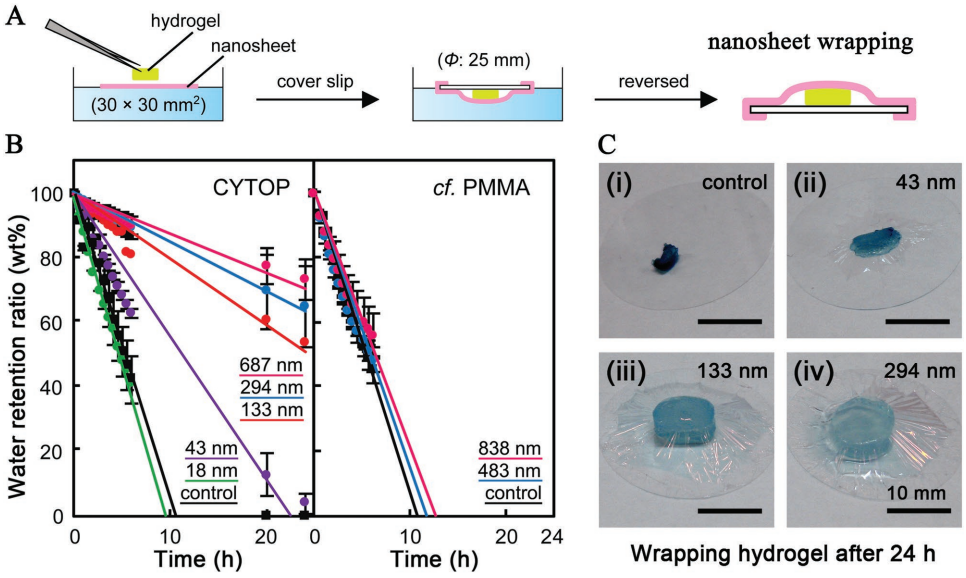


**Figure 2.** Characterization of water-retention effect of a CYTOP nanosheet. A) Schematic representation of sample wrapped with a nanosheet on the surface of water. B) Correlation between the water retention ratio and the time of test of CYTOP and PMMA nanosheets wrapping hydrogels with a variety of thicknesses (control group: without nanosheet wrapping). C) Macroscopic images of the hydrogels (blue dextran loaded) wrapped with CYTOP nanosheets of different thicknesses after 24 h.

concentration of coating solution, and adjustable in the range from 17.8 ± 0.2 to 686.6 ± 1.7 nm (Figure 1E). In all cases, the thickness deviation was less than 1%. In fact, the interference color of a CYTOP nanosheet was homogeneous across the entire $SiO_2$ substrate, and no striation pattern could be observed (Figure S1A, Supporting Information). However, the striation defect is much more obvious in a PMMA nanosheet with a similar thickness prepared from a chloroform solution (Figure S1B, Supporting Information). It is known that the radially oriented striation arises from a surface tension driven fluid flow, which is a common thickness nonuniformity defect in spin-coating films.[9] Here, the use of PFTBA with a high boiling point (≈180 °C) can prevent the appearance of striation and give a defect-free surface on CYTOP nanosheet. Moreover, we explored the relationship between adhesion strength and film thickness using a scratch tester. When a diamond tip horizontally gradually scratched the CYTOP nanosheet resupported on a $SiO_2$ substrate, the critical load at the detachment of nanosheet was recorded (Figure 1F). With a thickness decrease, the adhesion force markedly increased from $0.2 \times 10^5$ to $5.3 \times 10^5$ N $m^{-1}$, which is comparable to that of a vacuum deposited copper film (≈200 nm thickness) on a glass substrate.[10] Although the adhesion of nanosheets on moist tissue surfaces was not measured due to the experimental limitations, this results agrees very well with our previous study on PLLA nanosheets that indicated a thinner nanosheet has a higher potential to adhere.[5] Regarding transparency, a CYTOP nanosheet with thickness of 294.2 ± 1.5 nm had almost a 100% transmittance in the wavelength range from 200 to 800 nm (Figure 1G). This compares well to PMMA nanosheet, where the absorption in the middle-UV may restrict its application in biological microscopy.

As a model tissue sample, alginate hydrogel with a cylinder shape was employed. The hydrogel was gently placed in the center of a floated CYTOP nanosheet and covered with a piece of cover slip, which was then wrapped by the margin of nanosheet (**Figure 2**A). Nanosheets bent to produce wrinkles but were able to stand the weight of hydrogel and cover slip (≈500 mg in total) on the surface of water, owing to the high water surface tension and high stiffness/stretchability of CYTOP. By reversing the cover slip out of water surface, we discovered a tight adhesion between the surface of the hydrogel and the stretched CYTOP nanosheet. It should be noted that in some cases a certain amount of buffer was added. The existence of liquid does not weaken the adhesion between the sample and the cover slip as well as the nanosheet on both sides. In order to evaluate the water retention effect of the nanosheet, hydrogels containing blue dextran were wrapped with CYTOP or PMMA films with different thicknesses. Water in hydrogel (≈300 mg in total) evaporates at room temperature, and the water retention ratio can be calculated from the weight loss (Figure 2B). Without wrapping, the hydrogel became completely dehydrated after ≈10 h. When the hydrogels were wrapped with CYTOP nanosheets, evaporation was largely prevented. For instance, in the case of wrapping with a 133 nm thick CYTOP nanosheet, ≈60 wt% of water was retained even after 24 h. Such a water-retention effect was proportional to the CYTOP film thickness. This trend can be confirmed by observing the wrapped hydrogels as well, where the magnitude of shrinkage and the consequent dark color becomes obvious as the film thickness decreases (Figure 2C). In the case of PMMA films, while adhesion between the thick film and the hydrogel/cover slip remains high for a 24 h period (Figure S2, Supporting Information), the water-retention effect was negligible even when using a film over 800 nm in thickness. This test indicates that the CYTOP nanosheet-wrapped samples may keep fresh for a longer time and avoid the undesirable movement induced by the sample desiccation. Combined with the adhesion strength results, we believe that a CYTOP nanosheet with a thickness of 133 nm

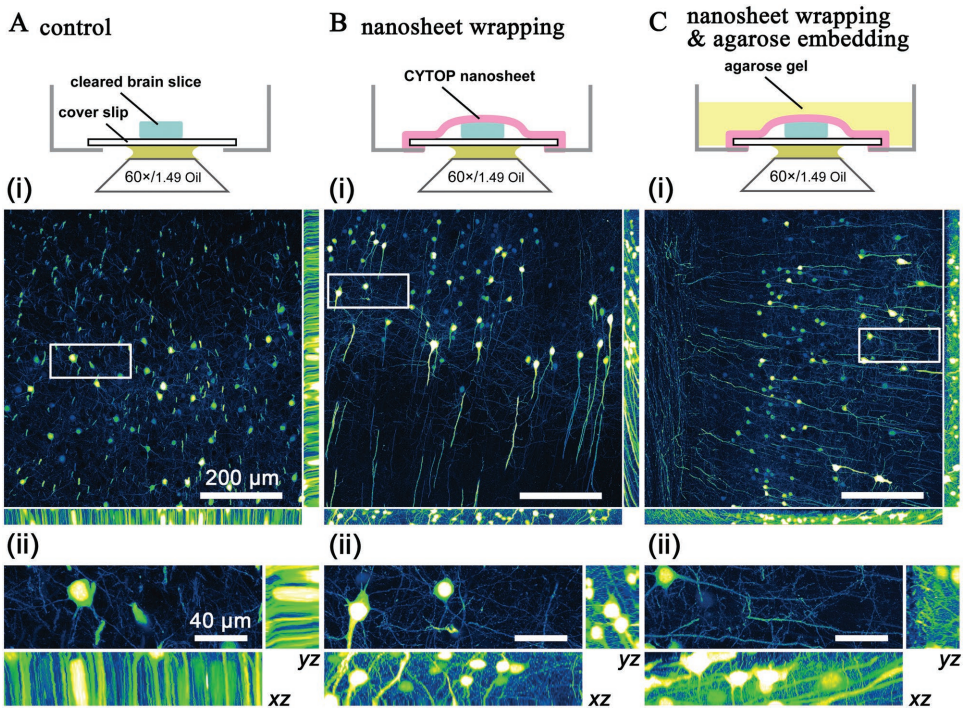


**Figure 3.** Confocal tissue imaging with tiled scaning of thy1-EYFP-H mouse brain slices. A–C) are projection images (maximum intensity projection) of cortical region taken from control (without nanosheet wrapping), with nanosheet wrapping, and with nanosheet wrapping combined with agarose embedding, respectively. Row (ii) are the corresponding magnified views of the highlighted regions in row (i). The schematic representations of the different mounting processes are provided above each column.

provides both sufficient water retention and surface adhesion for sample fixation, and is adopted in the following experiments if not otherwise specified. It should be noted that a firm adhesion of commercial plastic food wraps (≈10 μm thickness) to the cover slip cannot be achieved. The insufficient adhesion due to the micrometer scale thickness of plastic wraps always leads to undesirable detachment.

The performance of the nanosheet wrapping mount was finally evaluated in a practical tissue imaging setting. Cleared brain slices from thy1-EYFP-H transgenic mice expressing enhanced yellow fluorescent protein (EYFP) were used for the experiment.[11] This observation task is highly challenging due to the exquisite morphology of neuron cells. Even a slight sample movement can have an obvious adverse impact on the quality of imaging. Moreover, during a long-time observation, the ongoing evaporation causes locally nonuniform sample shrinkage, which results in a blurred image that cannot be filtered by post software processing. While agarose embedding can fix tissue samples and prevent evaporation to some extent, it is not applicable in this case. To the best of our knowledge, almost all the existing clearing treatments are reversible with diluted clearing agents. As shown in Figure S3 (Supporting Information), we verified that a Sca*l*eS treated brain slice would restore to its original nontransparent state after once contacting the water medium in the agarose cast solution. The poured agarose gel may also widen the gap between sample and cover slip, which decreases the achievable focus depth with a certain objective lens. In other words, agarose embedding destroys the cleared tissue samples and limits the depth of observation.

Here, Sca*l*eS cleared brain slices that were 1 mm thick were used for long-time and large area microscopic imaging in a tiling mode. Image stacks was acquired at a depth of about 40 to 44 μm with a 1 μm *z*-step over an area covering 761 × 756 μm with a stitching field of 4 × 4. For scans run at a moderate speed, generally the total observation time for one sample lasts for ≈2 h. With a certain sample mounting, the cortical region of the brain was arbitrarily chosen and the quality of imaging was analyzed. In a control group, the brain slice was directly observed without any wrapping fixation (**Figure 3**A). As expected, sample evaporation generated severe motion blur artifacts in the depth direction (*z* direction). In *xz* and *yz* projection images, the neuron body and axon fiber were elongated to a large extent and became unidentifiable. It is known that a typical neuron body is spherical shape with diameter varying from 5 to over 10 μm. We measured the 3D geometrical size of the neuron bodies and found an artificial average size of 12.5 ± 1.1, 32.3 ± 5.3, and 28.0 ± 6.6 μm in three directions ($n$ = 5). In addition, horizontal sample movement was observed as well, which was attributed to the nonuniform sample shrinkage as mentioned above. The irregular sample movement in $x$ or $y$ direction results in ghost artifacts in $xy$ projection images. And hence, to obtain a high quality tissue imaging, an appropriate mount is extremely important. The image of the cortical region taken with CYTOP nanosheet wrapping mount is shown in Figure 3B. It is clear that the brain slice was well fixed in both horizontal and vertical directions, due to the excellent water retention and good surface adhesion of nanosheet. The quality of imaging is

highly improved compared to the control group—a single axon fiber could indeed be identified. The measured neuron body size becomes much reasonable, that is, 11.9 ± 0.8, 11.2 ± 1.6, 11.7 ± 1.5 μm ($n$ = 5). It is worth noting that while wrapped with a 133 nm thick CYTOP nanosheet, sample evaporation cannot be prevented completely. For a continuous observation with a longer time span, such as 24 h, sample desiccation and shrinkage will still occur. Therefore, we also propose a combination of nanosheet wrapping and agarose embedding (Figure 3C). Here, the nanosheet acts as a barrier to block the water permeation from the agarose cast solution to the sample, and the cleared tissue will remain transparent during observation (Figure S3, Supporting Information). Similar to simple nanosheet wrapping, the combined mount exhibited a high spatial resolution in *xyz* directions as well. No visible artifacts arising from undesirable sample movement could be detected. The measured neuron body is 11.6 ± 2.0, 10.3 ± 2.3, 11.5 ± 2.2 μm in three directions ($n$ = 5). We believe that combined with agarose embedding, nanosheet wrapping can provide an ideal mount for long-time tissue imaging, while using just nanosheet wrapping is sufficient in most cases.

In conclusion, nanosheets composed of amorphous fluoropolymer CYTOP were prepared with adjustable thicknesses. Their excellent water retention and good surface adhesion lead us to propose a nanosheet wrapping mount that can be used on its own, or in combination with conventional agarose embedding. While the materials for building a wrapping mount are not limited to CYTOP and agarose, by wrapping with a 133 nm thick CYTOP nanosheet in this case study, we obtained a high spatial resolution and identifiability image of cleared mouse brain slices with a long-time scan over a large area. Although still at an early stage, this study establishes and verifies the superiority of nanosheet wrapping mounts for tissue imaging. In the future, as the refractive index of CYTOP is equivalent to that of water, we are planning to develop a glass-free nanosheet wrapping mount for deeper tissue imaging, which is expected to break the limit of the nominal working distance of a water immersion objective lens.

## Experimental Section

*Fabrication of Fluoropolymer Nanosheet*: Silicon wafers ($SiO_2$ substrate, KST World Co., Japan) cut into an appropriate size (typically 30 mm × 30 mm) were treated with a piranha solution, followed by rinsing with distilled water. PVA ($M_w$: 22 kDa, Kanto Chemical Co., Japan) was dissolved in water at 10 mg mL$^{-1}$. The solution was dropped onto the substrates and spin-coated at 4000 rpm for 20 s (Spin Coater MS-A100, Mikasa Co., Ltd. Japan). Next, a solution of CYTOP (CTX-809SP, Asahi Glass Co., Ltd. Japan) dissolved in PFTBA at a variety of concentrations (10–90 mg mL$^{-1}$) was dropped onto the PVA-coated substrates and spin-coated as described earlier. PMMA ($M_w$: 120 kDa, Sigma-Aldrich, USA) dissolved in chloroform was employed as coating solution as well. All the fabrication processes were conducted at room temperature (25 °C) and in a clean room (class 10 000 conditions).

*Characterization of Fluoropolymer Nanosheet*: The freestanding nanosheets were resupported on a required surface for the characterization. The thickness of nanosheets on $SiO_2$ substrate was analyzed by a stylus profilometer (DektakXT, Bruker Co., Germany). The morphology of CYTOP nanosheets on the Anodisc membrane (GE Healthcare, UK) was observed with a Hitachi S-4800 field emission SEM. The static water contact angle was obtained on a contact angle meter (DMe-201, Kyowa Interface Science Co., Ltd. Japan) at room temperature and a relative humidity of 40%. The adhesive strength of CYTOP nanosheets was measured by a scratch tester (CSR-2000, Rhesca Co., Ltd. Japan), as described in ref. [4a]. Regarding the optical transmittance, nanosheets were resupported on quartz glass, and the transmission spectrum was recorded with an UV–vis spectrophotometer (UV-3101PC, Shimadzu Co., Japan).

*Water-Retention Effect of Nanosheet*: Blue dextran ($M_w$: 2000 kDa, Sigma-Aldrich) containing sodium alginate (Kanto Chemical Co.) aqueous solution at 20 mg mL$^{-1}$ was poured into calcium chloride solution at 2 wt% with a ratio of 1:2 (v/v). An alginate hydrogel was formed after stirring overnight. Hydrogels to be wrapped were punched into a cylindrical shape with a diameter of 10 mm and thickness of 5 mm. Specifically, a hydrogel was gently placed in the center of a floated nanosheet on the surface of water. Using tweezers, a cover slip with a diameter of 25 mm (0.13–0.16 mm thickness, AS ONE Co., Japan) was pressed from above and then enfolded by the margin of the nanosheet. The original weight and weight of wrapped samples at certain time intervals over 24 h at room temperature and a relative humidity of 40% was measured as $W_0$ and $W_t$, respectively. Then, the sample was completely dried in an 80 °C oven and weight as $W_d$. The water retention ratio was thus obtained by $(W_t - W_d)/(W_0 - W_d) \times 100\%$.

*Preparation of Cleared Brain Slices and Mounting Process*: Thy1-EYFP-H transgenic mice were 8 to 12 weeks old at the time of viral infusion. The study was carried out in accordance with the recommendations in the Guidelines for the Care and Use of Laboratory Animals of the Animal Research Committee of Hokkaido University. All protocols were approved by the Institutional Animal Care and Use Committee of National University Corporation Hokkaido University (Permit Number: 14-0127). Fixed brains were removed and sliced using a Brain Matrices (Muromachi Kikai Co., Ltd. Japan) into 1 mm sections. These slices were cleared with the protocol of Sca*l*eS, as described in ref. [2b]. Slices with a piece of cover slip (25 mm diameter, 0.13–0.16 mm thickness) were wrapped with CYTOP nanosheet, and bonded to a perforated bottom dish (35 mm diameter) with nail enamel. In some cases, low melting point agarose (melting temperature ≤ 65 °C, Nacalai Tesque Inc. Japan) dissolved in PBS (pH 7.4) at 2.5 wt% was poured into the dish to embed the wrapped samples. As a control, the cleared brain slices were directly placed on the glass bottom dish for observation.

*Confocal Tissue Imaging of Brain Slices*: All the observations were performed with an inverted confocal microscope (A1R, Nikon Instruments Inc. Japan). Specifically, the mounted brain slice in a 35 mm dish was fixed on the sample stage. A 60× oil immersion objective lens (CFI Apochromat TIRF, numerical aperture (NA): 1.49, WD: 0.12 mm) and laser line at 514 nm were used. Fluorescent signals in the wavelength range of 500–550 nm were detected via a photomultiplier tube. Tiled scanning was applied for a large area and long-time observation. Image stacks was acquired at the depth about 40 to 44 μm with a 1 μm *z*-step, over an area covering 761 × 756 μm (3624 × 3600 pixels, 0.21 μm per pixel) with a stitching field of 4 × 4. The alignment of images, *xy*, *xz*, and *yz* projection images (maximum intensity projection) were generated through NIS-Elements AR software (ver. 4.60, Nikon Instruments Inc.).

## Supporting Information

Supporting Information is available from the Wiley Online Library or from the author.

## Acknowledgements

H.Z., A.M., and R.K. contributed equally to this work. The authors thank Prof. Shinji Takeoka at School of Advanced Science and Engineering, Waseda University for valuable discussions on scratch

 

tester for thin-films. Some of the experiments were conducted in Technical Service Coordination Office at Tokai University, Tokai University Imaging Center for Advanced Research (TICAR), and the Nikon Imaging Center (NIC) at Hokkaido University for technical assistance. This work was supported in part by a Grant-in-Aid for Scientific Research on Innovative Areas "Nanomedicine Molecular Science" (No. 2306) from the Ministry of Education, Culture, Sports, Science, and Technology of Japan (MEXT) (Y.O.), MEXT/JSPS KAKENHI Grant Number JP15H05953 "Resonance Bio" and JP26242082 (T.N.), a Grant-in-Aid for Matching Planner Program (No. MP27115663001) from the Japan Science and Technology Agency (Y.O., H.Z.), a MEXT-Supported Program for the Strategic Research Foundation at Private Universities (Y.O.), a FY2016 Cooperative Research Program (No. 20161027) and FY2017 Research Program of "Dynamic Alliance for Open Innovation Bridging Human, Environment and Materials" (No. 20173007) in "Network Joint Research Center for Materials and Devices" (Y.O., H.Z., R.K., T.N.).

## Conflict of Interest

The authors declare no conflict of interest.

## Keywords

agarose embedding, nanosheets, sample mounting, tissue imaging, wrapping

Received: June 6, 2017
Revised: July 5, 2017
Published online: August 11, 2017

[1] a) W. Denk, J. H. Strickler, W. W. Webb, *Science* **1990**, *248*, 73; b) P. J. Keller, A. D. Schmidt, J. Wittbrodt, E. H. K. Stelzer, *Science* **2008**, *322*, 1065; c) J. Huisken, J. Swoger, F. Del Bene, J. Wittbrodt, E. H. K. Stelzer, *Science* **2004**, *305*, 1007; d) S. W. Hell, J. Wichmann, *Opt. Lett.* **1994**, *19*, 780; e) M. J. Rust, M. Bates, X. Zhuang, *Nat. Methods* **2006**, *3*, 793; f) S. T. Hess, T. P. K. Girirajan, M. D. Mason, *Biophys. J.* **2006**, *91*, 4258.

[2] a) H. Hama, H. Kurokawa, H. Kawano, R. Ando, T. Shimogori, H. Noda, K. Fukami, A. Sakaue-Sawano, A. Miyawaki, *Nat. Neurosci.* **2011**, *14*, 1481; b) H. Hama, H. Hioki, K. Namiki, T. Hoshida, H. Kurokawa, F. Iswhidate, T. Kaneko, T. Akagi, T. Saito, T. Saido, A. Miyawaki, *Nat. Neurosci.* **2015**, *18*, 1518; c) A. Ertürk, K. Becker, N. Jährling, C. P. Mauch, C. D. Hojer, J. G. Egen, F. Hellal, F. Bradke, M. Sheng, H. U. Dodt, *Nat. Protoc.* **2012**, *7*, 1983; d) T. Kuwajima, A. A. Sitko, P. Bhansali, C. Jurgens, W. Guido, C. Mason, *Development* **2013**, *140*, 1364; e) K. Chung, J. Wallace, S. Y. Kim, S. Kalyanasundaram, A. S. Andalman, T. J. Davidson, J. J. Mirzabekov, K. A. Zalocusky, J. Mattis, A. K. Denisin, S. Park, H. Bernstein, C. Ramakrishnan, L. Grosenick, V. Gradinaru, K. Deisseroth, *Nature* **2013**, *497*, 332; f) M. T. Ke, S. Fujimoto, T. Imai, *Nat. Neurosci.* **2013**, *16*, 1154; g) E. A. Susaki, K. Tainaka, D. Perrin, F. Kishino, T. Tawara, T. M. Watanabe, C. Yokoyama, H. Onoe, M. Eguchi, S. Yamaguchi, T. Abe, H. Kiyonari, Y. Shimizu, A. Miyawaki, H. Yokota, H. R. Ueda, *Cell* **2014**, *157*, 726; h) Y. Aoyagi, R. Kawakami, H. Osanai, T. Hibi, T. Nemoto, *PLoS One* **2015**, *10*, 0116280.

[3] A. M. Glauert, *Fixation, Dehydration and Embedding of Biological Specimens*, Elsevier Science, Amsterdam, The Netherlands **1975**, pp. 73–110.

[4] a) C. Rossmann, E. Garrett-Mayer, F. Rattay, D. Haemmerich, *Physiol. Meas.* **2014**, *35*, 55; b) R. R. Boggio, D. A. Zaborske, C. N. Powers, *Lab. Med.* **1999**, *30*, 18; c) M. E. Dailey, E. Manders, D. R. Soll, M. Terasaki, in *Handbook of Biological Confocal Microscopy*, 3rd ed., (Ed: J. B. Pawley), Springer, New York **2006**, p. 394; d) S. Pentz, H. Horler, *J. Microsc.* **1992**, *167*, 97; e) M. E. Dailey, G. S. Marrs, D. Kurpius, *Cold Spring Harbor Protoc.* **2011**, *4*, 373; f) A. Ettinger, T. Wittmann, *Methods Cell Biol.* **2014**, *123*, 77.

[5] a) Y. Okamura, K. Kabata, M. Kinoshita, D. Saitoh, S. Takeoka, *Adv. Mater.* **2009**, *21*, 4388; b) Y. Okamura, K. Kabata, M. Kinoshita, H. Miyazaki, A. Saito, T. Fujie, S. Ohtsubo, D. Saitoh, S. Takeoka, *Adv. Mater.* **2013**, *25*, 545; c) T. Komachi, H. Sumiyoshi, Y. Inagaki, S. Takeoka, Y. Nagase, Y. Okamura, *J. Biomed. Mater. Res., Part B,* DOI: 10.1002/jbm.b.33714.

[6] R. R. Chao, S. S. H. Rizvi, in *ACS Symposium Series: Food and Packaging Interactions*, Vol. *365* (Ed: J. H. Hotchkiss), American Chemical Society, Washington, DC, USA **1988**, Ch. 18.

[7] J. G. Drobny, *Technology of Fluoropolymers*, 2nd ed., CRC Press, Boca Raton, FL, USA **2009**, pp. 151–153.

[8] a) C. S. Lee, S. H. Lee, S. S. Park, Y. K. Kim, B. G. Kim, *Biosens. Bioelectron.* **2003**, *18*, 437; b) L. J. Cheng, M. T. Kao, E. Meyhöfer, L. J. Guo, *Small* **2005**, *1*, 409; c) X. Cheng, M. Caironi, Y. Y. Hoh, J. Wang, C. Newman, H. Yan, A. Facchetti, H. Sirringhaus, *Chem. Mater.* **2010**, *22*, 1559; d) D. K. Hwang, C. Fuentes-Hernandez, J. Kim, W. J. Potscavage Jr., S. J. Kim, B. Kippelen, *Adv. Mater.* **2011**, *23*, 1293; e) S. Yang, T. N. Krupenkin, P. Mach, E. A. Chandross, *Adv. Mater.* **2003**, *15*, 940.

[9] a) D. P. Birnie III, *J. Mater. Res.* **2001**, *16*, 1145; b) D. E. Haas, D. P. Birnie III, M. J. Zecchino, J. T. Figueroa, *J. Mater. Sci. Lett.* **2001**, *20*, 1763; c) N. Bassou, Y. Rharbi, *Langmuir* **2009**, *25*, 624; d) P. D. Fowler, C. Ruscher, J. D. McGraw, J. A. Forrest, K. Dalnoki-Veress, *Eur. Phys. J. E* **2016**, *39*, 90.

[10] S. Baba, T. Midorikawa, T. Nakano, *Appl. Surf. Sci.* **1999**, *344*, 144.

[11] G. Feng, R. H. Mellor, M. Bernstein, C. Keller-Peck, Q. T. Nguyen, M. Wallace, J. M. Nerbonne, J. W. Lichtman, J. R. Sanes, *Neuron* **2000**, *28*, 41.

 